Received: 8 July 2023 | Revised: 19 December 2023 | Accepted: 12 April 2024

IET Power Electronics

DOI: 10.1049/pel2.12707

The Institution of Engineering and Technology WILEY

ORIGINAL RESEARCH

Predictive power control strategy without grid voltage sensors of the Vienna rectifier

Tao Yang[1] | **Lan Chen**[2] | **Yiru Miao**[2]

[1]School of Rail Transit and Aviation Service, Chongqing Industry Polytechnic College, Chongqing, China

[2]State Key Laboratory of Power Transmission Equipment and System Security and New Technology, Chongqing University, Chongqing, China

Correspondence
Tao Yang, School of Rail Transit and Aviation Service, Chongqing Industry Polytechnic College, Chongqing, China.
Email: justmuch@qq.com

Funding information
Science and Technology Research Program of Chongqing Municipal Education Commission, Grant/Award Number: KJQN202203221; Doctoral Research Foundation of Chongqing Industry Polytechnic College, Grant/Award Number: 2022GZYBSZK1-04

Abstract

This paper proposes a predictive power control strategy for the three-phase, six-switch Vienna rectifier without grid voltage sensors to reduce the hardware cost and complexity of a high-power PWM rectifier system. Firstly, an algorithm for calculating the AC-side voltage in the $\alpha\beta$ coordinate system is derived according to the operating principle of the Vienna rectifier, and a voltage observer is constructed by combining a second-order low-pass filter to estimate the grid voltage. Secondly, a soft start method is designed to solve the problem that the rectifier is prone to inrush current when it is started. Furthermore, the control method of grid voltage sensorless is combined with predictive power control with good dynamic characteristics and simple parameter settings to form the control strategy proposed in this paper. Finally, simulation analysis and experimental verification are carried out on the proposed control strategy. Simulation and experimental results show that the grid voltage estimation has high accuracy, a good surge current suppression effect, unit power factor operation, low input current harmonic content, and good dynamic and steady-state performance. Therefore, the correctness and effectiveness of the strategy proposed in this paper are verified.

1 | INTRODUCTION

The three-phase Vienna rectifier has drawn the attention of both industry and academia due to its numerous benefits, including no requirement for setting dead time, reduced switch tube stress, low harmonic content of grid-side current, and high efficiency. It is a topology with a wide range of application prospects [1–3].

Presently, the control strategy of the Vienna rectifier can be mainly categorized into power control and current control. Although these two control strategies differ in their dynamic characteristics and control effect, they both necessitate the accurate acquisition of the grid voltage to establish a closed-loop feedback system [3, 4]. In practical applications, a voltage sensor is often deployed to sample the grid voltage, which results in increased size, cost and hardware complexity. In addition, sensing the signals from sensors may cause noise and interference, and occasional faults and detection errors will also significantly degrade the performance of control system [5].

To enhance the reliability of the rectifier, several scholars have conducted related research on grid voltage sensorless. A control algorithm without grid voltage sensors based on the instantaneous power theory is proposed in [6]. However, this algorithm is susceptible to high-frequency noise interference due to the differential operation of the current. Therefore, various grid voltage estimation methods have been proposed, such as Kalman filter [7], state observer [8], neural network estimation [9], and so on. However, some practical problems occur with the above methods, such as difficulty in parameter setting and complicated calculations. A control strategy of grid voltage sensorless based on virtual flux linkage technology for three-phase voltage source PWM rectifiers is proposed in [10], which can effectively suppress the influence of grid voltage harmonics on the system. The algorithm is simple, but there are initial values and a direct current (DC) bias problem. In flux observation of an alternating current (AC) motor, a first-order low-pass filter is often used to replace the pure integral item, but this method will cause phase delay and amplitude error. To this end, a resonant filter based on the principle of virtual magnetic flux is proposed in [11] for the three-phase PWM rectifier, and a virtual magnetic flux compensation algorithm is designed to compensate for the magnetic flux delay. A sliding mode

variable structure technology is used in [12] to estimate the grid-side voltage, and an adaptive compensation is designed for compensating flux linkage for the integration part, which can effectively suppress the grid-side high-frequency harmonics and the transient oscillation of the DC-side output voltage. A photovoltaic grid-connected system is studied in [13], and the idea that a third-order integrator is used to estimate the flux linkage is proposed. By adjusting the DC bus voltage, the power conversion between the pump drive and the public power drive direction is realized, and the number of sensors is reduced. The absolute value of the input current is used in [14] to estimate the grid voltage for the three-phase, three-switch Vienna rectifier. Since the grid voltage information is not needed, the system's reliability is improved, but the dynamic performance is reduced at the same time. The control effectively without grid voltage sensors of the three-phase Vienna rectifier under the input current-oriented coordinate system is realized in [15].

Currently, there are few research studies on predictive control strategies for grid voltage sensorless. A grid voltage sensorless control method based on virtual flux linkage and deadbeat predictive direct control is proposed in [16], but it has the shortcomings of high switching frequency and poor robustness. A model predictive power control based on a sliding mode observer is proposed in [17]. The requirement for the accuracy of grid voltage estimation is increased for consideration of the unbalanced state of the grid. A band-pass filter and model reference adaptive system observer are used in [18] to solve the problem of current differentiation and model parameter accuracy. Since the adaptive function needs to be obtained according to Lyapunov's theory, the process of calculation is complicated.

Most of the aforementioned papers are focused on three-phase voltage source type PWM rectifiers, and there are many unsystematic researches on three-phase, three-level PWM rectifiers. As a three-phase Vienna rectifier with a more complex topology and control, it is necessary to ensure the accuracy of the calculation while taking into account the simplicity of the acquisition of the AC-side voltage value.

The start-up procedure of the rectifier is a crucial aspect of the control system; however, limited literature is available on this subject [19]. In [20], a resistor and a switch in series on the AC side are employed to restrict the initial current amplitude and facilitate pre-charging by progressively advancing the duty cycle of the lower bridge-arm switch tubes. [21] suggested governing the switch tubes of the corresponding phases based on different sectors and transitioning to the PWM rectification strategy upon the gradual ascent of the output voltage to the reference value. The aforementioned two methods directly regulate the switching devices, thus elevating the electrical stress on some components and potentially impacting their lifespan. In [22], the rectifier is made to operate in its natural rectification state before initiating the drive signals of the switching tubes, with the input current used to assess the phase angle of the grid voltage, successfully evading the start-up overcurrent issue. In [23], a three-step start-up approach is proposed, guaranteeing that the inrush current of the three-phase six-switch rectifier stays beneath a pre-designated threshold while also presenting no overshoot when the output voltage elevates to the reference value.

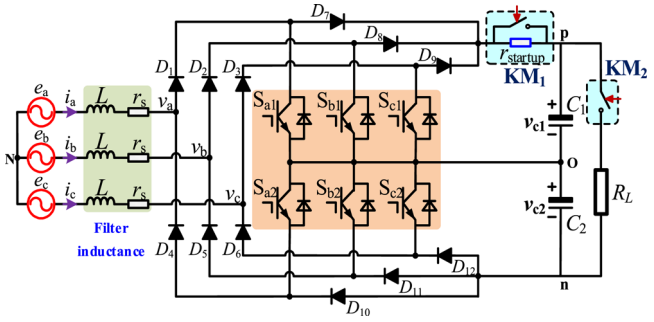

FIGURE 1 Topology of three-phase six-switch Vienna rectifier.

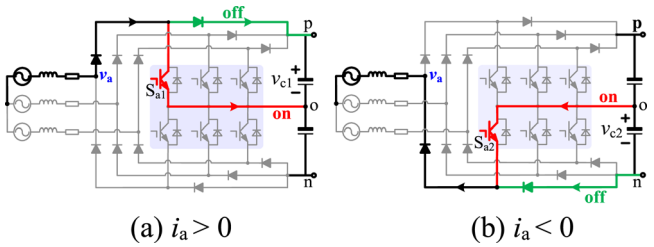

FIGURE 2 Working conditions of the Vienna rectifier.

This paper presents a grid voltage sensor-free control method for the three-phase six-switch Vienna rectifier. Firstly, an algorithm is derived for estimating the AC-side voltage based on the working principle of the rectifier. Secondly, a predictive power control strategy is introduced, where the instantaneous power is computed using the instantaneous power theory and the power tracking error is minimized as the objective. This leads to a predictive power control strategy that doesn't require a grid voltage sensor for the three-phase Vienna rectifier. Moreover, a soft-start control strategy is designed to address the issue of excessive start-up impulse current in the Vienna rectifier system. Finally, a MATLAB/Simulink simulation model and experimental prototype are developed to validate the proposed control strategy, which is proven to be correct and effective.

2 | WORKING PRINCIPLE OF THREE-PHASE SIX-SWITCH VIENNA RECTIFIER

The topology of the three-phase, six-switch Vienna rectifier is shown in Figure 1. e_a, e_b, and e_c are the three-phase grid voltage; i_a, i_b. i_c are the three-phase input currents. L is the filter inductance. r_s is the equivalent resistance of the filter inductance. v_a, v_b, and v_c are the AC-side voltage; $D_1 \sim D_6$ are rectifier diodes. $D_7 \sim D_{12}$ are fast-recovery freewheeling diodes. S_{ij} (i = a, b, c; j = 1, 2) are six power switching tubes; C_1 and C_2 are DC-side split capacitors. R_L is the resistive load. KM_1 and KM_2 are relays. $r_{start\text{-}up}$ is a current-limiting resistance.

Take phase A as an example to analyze the working principle of the rectifier: when the input current $i_a > 0$, due to the reverse blocking effect of D_4, it can only be controlled by S_{a1} at this time, as shown in Figure 2a. Ignoring the conduction loss of diodes, $v_a = v_{c1}$ when S_{a1} is off; $v_a = 0$ when S_{a1} is on.

TABLE 1 The relation among the switch quantities.

S_i	i_i	s_i	s_{io}	s_{ip}	s_{in}
$S_{i1,2}$ is on	/	Potential o	1	0	0
S_{i1} is off	> 0	Potential p	0	1	0
S_{i2} is off	> 0	Potential n	0	0	1

When the input current $i_a < 0$, due to the reverse blocking effect of D_1, it can only be controlled by S_{a2} at this time, as shown in Figure 2b. Similarly, $v_a = -v_{c2}$ when S_{a2} is off, and $v_a = 0$ when S_{a2} is on.

3 | ESTIMATION METHOD OF GRID VOLTAGE FOR VIENNA RECTIFIER

3.1 | Estimation method of AC-side voltage

Based on the operational principle of the Vienna rectifier, the switch tubes of the three-phase bridge arm can be modelled as a three-valued logic switching function:

$$s_i = \begin{cases} \text{o } S_{i1} \text{ or } S_{i2} \text{ conduction} \\ \text{p } S_{i1} \text{ turn off} \quad i_i > 0 \\ \text{n } S_{i2} \text{ turn off} \quad i_i < 0 \end{cases} \tag{1}$$

where s_i is the potential state of the AC-side voltage of the ith phase; S_{i1} and S_{i2} are the switch tubes of the ith phase and i_i is the current of the ith phase.

The s_i can be equivalent to three switches: s_{io}, s_{ip}, and s_{in}. When the switch is turned on, its value is recorded as 1; when it is turned off, it is recorded as 0. Thus, the relationship in Table 1 can be obtained.

The mathematical model of the three-phase Vienna rectifier in the three-phase stationary coordinate system can be expressed as:

$$\begin{bmatrix} e_a \\ e_b \\ e_c \end{bmatrix} = r_s \begin{bmatrix} i_a \\ i_b \\ i_c \end{bmatrix} + L\frac{d}{dt}\begin{bmatrix} i_a \\ i_b \\ i_c \end{bmatrix} + \begin{bmatrix} v_{ao} \\ v_{bo} \\ v_{co} \end{bmatrix} + v_{oN} \tag{2}$$

where v_{ao}, v_{bo}, and v_{co}, are the voltage differences between nodes a, b, c, and o, respectively; v_{oN} is the voltage difference between points o and N.

The relationship between the AC-side voltage and the neutral-point voltage of the DC-side capacitor can be obtained based on the working principle of the Vienna rectifier:

$$\begin{cases} v_{ao} = s_{ap}v_{c1} - s_{an}v_{c2} \\ v_{bo} = s_{bp}v_{c1} - s_{bn}v_{c2} \\ v_{co} = s_{cp}v_{c1} - s_{cn}v_{c2} \end{cases} \tag{3}$$

Assuming that the three-phase grid voltage is symmetrical, the relationship between the three phases on the AC side is as follows:

$$\begin{cases} e_a + e_b + e_c = 0 \\ i_a + i_b + i_c = 0 \end{cases} \tag{4}$$

Substituting formulas (3) and (4) into formula (2), the expression for v_{oN} can be derived as formula (5):

$$v_{oN} = -\frac{1}{3}\left[\sum_{i=a,b,c} s_{ip}v_{c1} - \sum_{i=a,b,c} s_{in}v_{c2}\right] \tag{5}$$

By adding formulas (3) and (5), formula (6) can be obtained:

$$\begin{bmatrix} v_a \\ v_b \\ v_c \end{bmatrix} = v_{c1}\begin{bmatrix} s_{ap} - X \\ s_{bp} - X \\ s_{cp} - X \end{bmatrix} + v_{c2}\begin{bmatrix} -s_{an} + Y \\ -s_{bn} + Y \\ -s_{cn} + Y \end{bmatrix} \tag{6}$$

where $X = \frac{1}{3}\sum_{i=a,b,c} s_{ip}$ and $Y = \frac{1}{3}\sum_{i=a,b,c} s_{in}$.

Carrying out the Clarke transformation of formula (6), the estimated value of the AC-side voltage in the two-phase stationary coordinate system can be obtained:

$$\begin{bmatrix} v_\alpha \\ v_\beta \end{bmatrix} = \begin{bmatrix} \frac{2}{3} & -\frac{1}{3} & -\frac{1}{3} \\ 0 & \frac{\sqrt{3}}{3} & -\frac{\sqrt{3}}{3} \end{bmatrix}\begin{bmatrix} v_a \\ v_b \\ v_c \end{bmatrix} \tag{7}$$

3.2 | Estimation method of grid voltage

The mathematical model of the three-phase, six-switch Vienna rectifier in the two-phase stationary coordinate system is described as follows:

$$\begin{bmatrix} e_\alpha \\ e_\beta \end{bmatrix} = r_s\begin{bmatrix} i_\alpha \\ i_\beta \end{bmatrix} + L\frac{d}{dt}\begin{bmatrix} i_\alpha \\ i_\beta \end{bmatrix} + \begin{bmatrix} v_\alpha \\ v_\beta \end{bmatrix} \tag{8}$$

where e_α, e_β, i_α, i_β, v_α, v_β are the grid voltage, grid current, and inverter side voltage, respectively.

However, in practical applications, variations in the voltage drop across semiconductor power devices, inductance changes with operating conditions, and other non-ideal factors can all contribute to inaccuracies in formula (8), which will lead to the estimation errors of e_α and e_β. In order to address these potential discrepancies, the extended state observer (ESO) is employed to estimate the disturbances. The lumped disturbances are used to represent all variations and are named as F_α and F_β. At this point, formula (8) is rewritten as:

$$\begin{cases} \frac{d}{dt}\begin{bmatrix} i_\alpha \\ i_\beta \end{bmatrix} = -\frac{r_s}{L}\begin{bmatrix} i_\alpha \\ i_\beta \end{bmatrix} - \frac{1}{L}\begin{bmatrix} v_\alpha \\ v_\beta \end{bmatrix} + \frac{1}{L}\begin{bmatrix} e_\alpha \\ e_\beta \end{bmatrix} + \begin{bmatrix} F_\alpha \\ F_\beta \end{bmatrix} \\ \frac{d}{dt}\begin{bmatrix} F_\alpha \\ F_\beta \end{bmatrix} = \begin{bmatrix} R_\alpha \\ R_\beta \end{bmatrix} \end{cases} \tag{9}$$

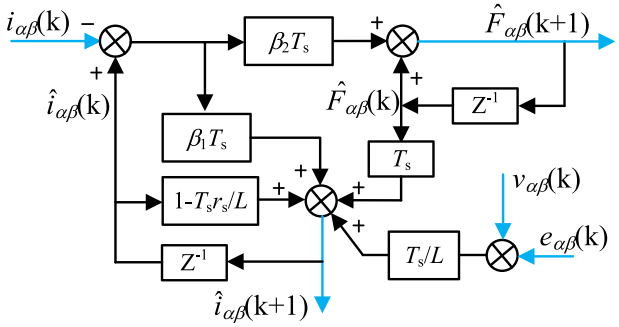

FIGURE 3 Discrete block diagram of proposed ESO.

where R_α and R_β are the variation rates of the disturbance. Based on this, the ESO can be designed as follows:

$$\begin{cases} err_{\alpha\beta} = \hat{i}_{\alpha\beta} - i_{\alpha\beta} \\ \dfrac{\mathrm{d}}{\mathrm{d}t}\hat{i}_{\alpha\beta} = -\dfrac{r_s}{L}\hat{i}_{\alpha\beta} - \dfrac{1}{L}v_{\alpha\beta} + \dfrac{1}{L}e_{\alpha\beta} + \hat{F}_{\alpha\beta} + \beta_1 err_{\alpha\beta} \\ \dfrac{\mathrm{d}}{\mathrm{d}t}\hat{F}_{\alpha\beta} = \beta_2 err_{\alpha\beta} \end{cases} \tag{10}$$

where β_1 and β_2 are the coefficients of ESO. According to formula (10), the characteristic equation of the ESO can be expressed as:

$$s^2 + \left(\frac{r_s}{L} - \beta_1\right)s - \beta_2 = 0 \tag{11}$$

To ensure that ESO is stable, the root of formula (11) should be negative, and the coefficient of ESO can be obtained as:

$$\begin{cases} \beta_1 = \dfrac{r_s}{L} - 2\omega_n \\ \beta_2 = -\omega_n^2 \end{cases} \tag{12}$$

where ω_n is the undamped natural frequency associated with the ESO bandwidth. It should be noted that increasing bandwidth ω_n can improve the ESO estimation speed however, this improvement comes at the cost of introducing more measurement noise. According to the measured noise level and the expected estimation rate, the value of ω_n is set as 100 Hz in this paper. The discretized forms of formula (10) are obtained as follows:

$$\begin{cases} err_{\alpha\beta}(k) = \hat{i}_{\alpha\beta}(k) - i_{\alpha\beta}(k) \\ \hat{i}_{\alpha\beta}(k+1) = \left(1 - \dfrac{r_s}{L}T_s\right)\hat{i}_{\alpha\beta}(k) - \dfrac{T_s}{L}v_{\alpha\beta}(k) + \dfrac{T_s}{L}e_{\alpha\beta}(k) \\ \qquad\qquad + T_s\hat{F}_{\alpha\beta}(k) + T_s\beta_1 err_{\alpha\beta}(k) \\ \hat{F}_{\alpha\beta}(k+1) = \hat{F}_{\alpha\beta}(k) + T_s\beta_2 err_{\alpha\beta} \end{cases} \tag{13}$$

where k denotes the sampling amount at k time, k+1 denotes the sampling amount at k+1 time, and T_s is the sampling period. Therefore, the control block diagram of ESO is shown in Figure 3.

The grid voltage of the Vienna rectifier can be estimated by formula (9). However, the presence of differential operations in the formula may lead to high sensitivity to noise. To mitigate this, the integral operation is performed on both sides of formula (9):

$$\begin{bmatrix} \int e_\alpha \mathrm{d}t \\ \int e_\beta \mathrm{d}t \end{bmatrix} = r_s \begin{bmatrix} \int i_\alpha \mathrm{d}t \\ \int i_\beta \mathrm{d}t \end{bmatrix} + L\begin{bmatrix} i_\alpha \\ i_\beta \end{bmatrix} + \begin{bmatrix} \int v_\alpha - L\hat{F}_\alpha \mathrm{d}t \\ \int v_\beta - L\hat{F}_\beta \mathrm{d}t \end{bmatrix} \tag{14}$$

In the two-phase stationary coordinate system, there are the following relations:

$$\begin{bmatrix} z_\alpha \\ z_\beta \end{bmatrix} = \omega \begin{bmatrix} -\int z_\beta \mathrm{d}t \\ \int z_\alpha \mathrm{d}t \end{bmatrix} \tag{15}$$

where z represents e or i.

By combining formulas (14) and (15), the estimation formula for the grid voltage can be deduced as formula (16):

$$\begin{bmatrix} e_\alpha \\ e_\beta \end{bmatrix} = r_s \begin{bmatrix} i_\alpha \\ i_\beta \end{bmatrix} + \omega L \begin{bmatrix} -i_\beta \\ i_\alpha \end{bmatrix} + \omega \begin{bmatrix} -\int v_\beta - L\hat{F}_\beta \mathrm{d}t \\ \int v_\alpha - L\hat{F}_\alpha \mathrm{d}t \end{bmatrix} \tag{16}$$

In formula (16), the differential operation is omitted, and a pure integral link is introduced, which poses problems with respect to the initial value and offset. If left unsolved, this may result in higher inrush currents. Based on the characteristic of integration, the amplitude of the AC-side voltage attenuates to $1/\omega$ times after integration, and the phase shift is $-\pi/2$.

For a second-order low-pass filter with a gain $K = 2$, its input-output characteristic exhibits: when the frequency ω of the input signal equals the cut-off frequency ω_c, the amplitude of the output signal remains unchanged and the phase shift is $-\pi/2$. The transfer function is expressed as follows:

$$G(s) = \frac{2\omega_c^2}{s^2 + 2\omega_c s + \omega_c^2} \tag{17}$$

where $\omega_c = 100\pi$ rad/s.

The Bode plots for the first-order filter, the pure integral term, and the second-order filter are illustrated in Figure 4. At a frequency of 50 Hz, the phase of the second-order filter is $-\pi/2$, identical to that of the pure integral term, whereas the amplitude of the second-order filter is 0 dB. Therefore, the proposed second-order low-pass filter with gain $K = 2$ can substitute for the pure integral term.

An improved grid voltage observer based on a second-order low-pass filter is proposed on the basis of formulas (16) and (17), which can effectively avoid pure integral operation. Its block diagram is illustrated in Figure 5.

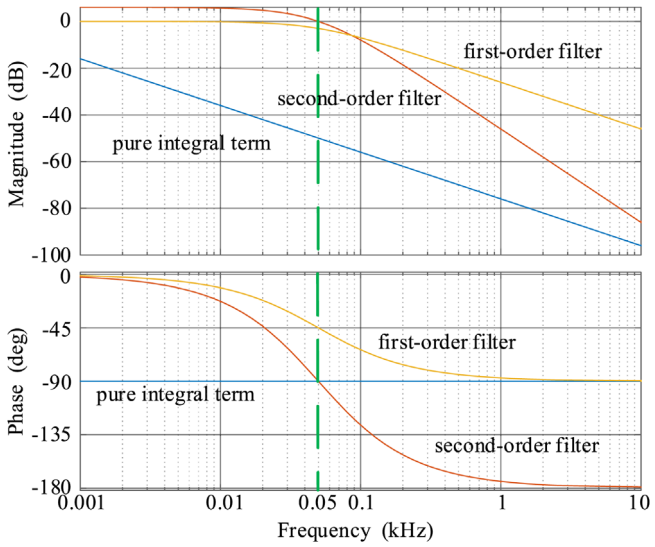

FIGURE 4 The Bode plots of the first-order filter, the pure integral term and the second-order filter.

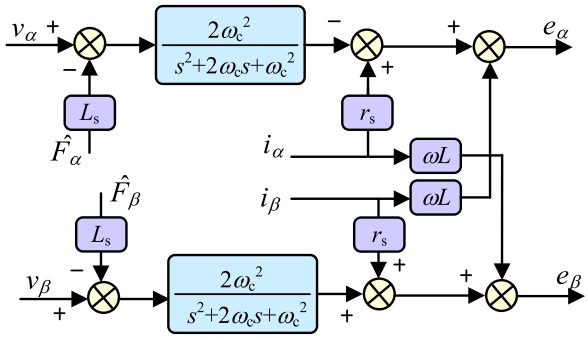

FIGURE 5 Structure diagram of grid voltage observer.

Considering the application of second-order filters in digital processor, the Tustin method is used to discretize second-order filter. The discretized second-order filter can be described as:

$$G(z) = \frac{N_1(z^2 + 2z + 1)}{D_1 z^2 + D_2 z + D_3} \tag{18}$$

where $N_1 = 2\omega_c{}^2 T_s{}^2$, $D_1 = 4+\omega_c{}^2 T_s{}^2+4\omega_c T_s$, $D_2 = 2\omega_c{}^2 T_s{}^2-8$ and $D_3 = 4+\omega_c{}^2 T_s{}^2-4\omega_c T_s$. If the AC side voltage integral at time k is expressed as $m(k)$, the following expression can be derived:

$$\begin{aligned} m(k) = {} & \frac{N_1}{D_1} v_\beta(k) + \frac{2N_1}{D_1} v_\beta(k-1) + \frac{N_1}{D_1} v_\beta(k-2) \\ & - \frac{D_2}{D_1} m(k-1) - \frac{D_3}{D_1} m(k-2) \end{aligned} \tag{19}$$

According to the above derivation process, the flow chart of the estimation algorithm of grid voltage proposed in this paper can be constructed, as shown in Figure 6.

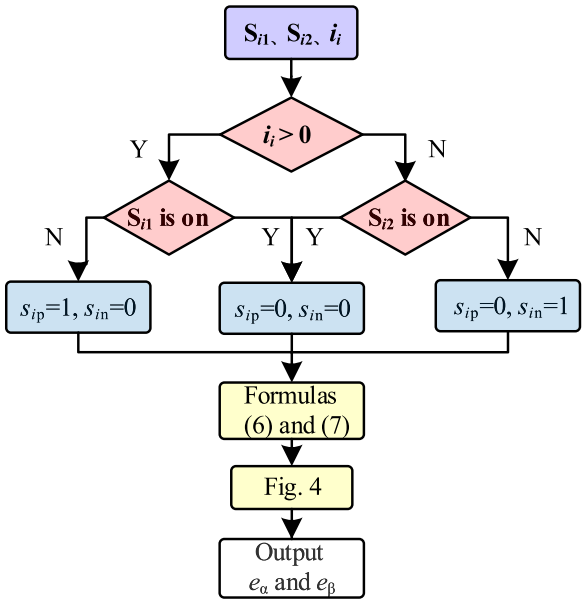

FIGURE 6 Flow chart of grid voltage estimation algorithm.

4 | SUPPRESSION METHOD OF IMPULSE CURRENT

Due to the significant difference between the reference value (v_{dcref}) and the actual value of the DC-side output voltage (v_{dc}) during the startup of the Vienna rectifier, a proportional integral (PI) regulator is used to increase the active power reference value P_{ref} and the instantaneous active power rapidly, resulting in a relatively large impulse current. To address this issue, a soft-start strategy is proposed in this paper, which includes two stages:

Stage 1: The rectifier operates in uncontrolled rectification mode, in which all power switch tubes S_{ij} and relays KM_1 and KM_2 are in the off state. The current-limiting effect of the resistor $r_{start\text{-}up}$ effectively suppresses the impulse current during this stage. After 0.13s, the DC-side capacitor voltage rises to the preset value, indicating the readiness to enter stage 2.

Stage 2: The rectifier switches to PWM rectification mode, and the relays KM_1 and KM_2 are closed. Given the significant difference between the output voltage and its reference value (700 V) at the end of stage 1, a gentle curve function is used as the reference value, gradually increasing up to 700 V to reduce the difference between the output voltage and its reference value and suppress the impulse current during this stage. The slope of the gentle curve function is better within the range of $515/0.13 \le k \le 700/0.13$. Figure 7 demonstrates the transition process of the output voltage with different slope values, taking into account the magnitude of the impulse current, the output voltage process, and the required time. Considering all factors, the slope of the gentle curve function is ultimately set at $k = 4550$.

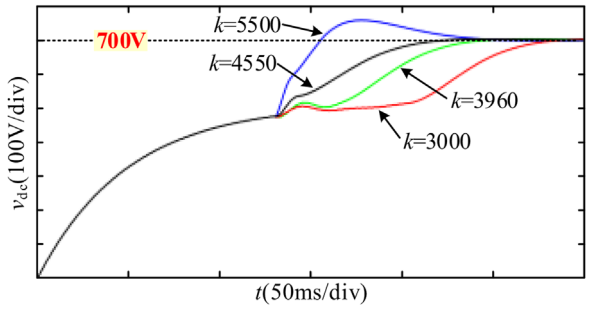

FIGURE 7 Output voltage waveform with different k values during start-up processes.

5 | PREDICTIVE POWER CONTROL STRATEGY OF VIENNA RECTIFIER

In the two-phase stationary coordinate system, the formula for calculating the instantaneous power of the three-phase Vienna rectifier is given by formula (20):

$$\begin{bmatrix} P \\ Q \end{bmatrix} = \begin{bmatrix} e_\alpha & e_\beta \\ e_\beta & -e_\alpha \end{bmatrix} \begin{bmatrix} i_\alpha \\ i_\beta \end{bmatrix} \tag{20}$$

Subsequently, by performing a differential operation on formula (20), formula (21) can be derived:

$$\frac{d}{dt}\begin{bmatrix} P \\ Q \end{bmatrix} = \begin{bmatrix} e_\alpha & e_\beta \\ e_\beta & -e_\alpha \end{bmatrix} \cdot \frac{d}{dt}\begin{bmatrix} i_\alpha \\ i_\beta \end{bmatrix} + \begin{bmatrix} i_\alpha & i_\beta \\ -i_\beta & i_\alpha \end{bmatrix} \cdot \frac{d}{dt}\begin{bmatrix} e_\alpha \\ e_\beta \end{bmatrix} \tag{21}$$

The relationship between the grid voltage vectors in the two-phase stationary coordinate system is represented by formula (22):

$$\frac{d}{dt}\begin{bmatrix} e_\alpha \\ e_\beta \end{bmatrix} = \omega \begin{bmatrix} -e_\beta \\ e_\alpha \end{bmatrix} \tag{22}$$

By incorporating the formulas (8), (21), and (22), and neglecting the influence of r_s, the rate of change of instantaneous power is determined by formula (23):

$$\begin{cases} \dfrac{dP}{dt} = \dfrac{e_\alpha^2 + e_\beta^2 - e_\alpha v_\alpha - e_\beta v_\beta}{L} - \omega Q \\ \dfrac{dQ}{dt} = \dfrac{e_\alpha v_\beta - e_\beta v_\alpha}{L} + \omega P \end{cases} \tag{23}$$

Since the system sampling period T_s is much shorter compared to the grid fundamental wave period, the instantaneous power can be discretized within a sampling period by applying formula (24):

$$\begin{cases} \dfrac{dP}{dt} = \dfrac{P(k+1) - P(k)}{T_s} \\ \dfrac{dQ}{dt} = \dfrac{Q(k+1) - Q(k)}{T_s} \end{cases} \tag{24}$$

Substituting formula (23) in formula (24) and carrying out necessary transformations, the formula (25) is obtained:

$$\begin{cases} P(k+1) = P(k) - \omega T_s Q(k) + \dfrac{T_s}{L}\left(e_\alpha^2 + e_\beta^2 - e_\alpha v_\alpha - e_\beta v_\beta\right) \\ Q(k+1) = Q(k) + \omega T_s P(k) + \dfrac{T_s}{L}\left(e_\alpha v_\beta - e_\beta v_\alpha\right) \end{cases} \tag{25}$$

According to the theory of predictive power control, ensuring the minimum power tracking error at the end of each period is necessary to obtain the desired AC-side voltage vector (v_α, v_β) of the rectifier. Therefore, the objective function can be defined as:

$$F = \Delta P^2 + \Delta Q^2 \tag{26}$$

where ΔP and ΔQ are the difference values between the reference values (P_{ref}, Q_{ref}) of instantaneous power and their predicted values ($P_{(k+1)}$, $Q_{(k+1)}$), respectively. Substituting (25) into (26), the objective function F can be expressed in detail.

$$\begin{aligned} F = &\left[P_{ref} - P + \omega T_s Q - \frac{T_s}{L}(e_\alpha^2 + e_\beta^2 - e_\alpha v_\alpha - e_\beta v_\beta)\right]^2 \\ &+ \left[Q_{ref} - Q - \omega T_s P - \frac{T_s}{L}(e_\alpha v_\beta - e_\beta v_\alpha)\right]^2 \end{aligned} \tag{27}$$

Calculating $\frac{\partial F}{\partial v_\alpha}$ and $\frac{\partial F}{\partial v_\beta}$ respectively.

$$\begin{cases} \dfrac{\partial F}{\partial v_\alpha} = Ae_\alpha + Be_\beta - \dfrac{T_s}{L}\left\|e_{\alpha\beta}\right\|^2 (e_\alpha - v_\alpha) \\ \dfrac{\partial F}{\partial v_\beta} = Ae_\beta - Be_\alpha - \dfrac{T_s}{L}\left\|e_{\alpha\beta}\right\|^2 (e_\beta - v_\beta) \end{cases} \tag{28}$$

It is obvious that there is only one minimum value in F. $\frac{\partial F}{\partial v_\alpha} = 0$ and $\frac{\partial F}{\partial v_\beta} = 0$ need to be satisfied to minimize the tracking error of instantaneous power, so formula (29) can be derived:

$$\begin{cases} v_\alpha = e_\alpha - \dfrac{L}{T_s\|e_{\text{fffi}}\|^2}\left(\text{A}e_\alpha + \text{B}e_\beta\right) \\ v_\beta = e_\beta - \dfrac{L}{T_s\|e_{\text{fffi}}\|^2}\left(\text{A}e_\beta - \text{B}e_\alpha\right) \end{cases} \tag{29}$$

where $\|e_{\text{fffi}}\| = \sqrt{e_\alpha^2 + e_\beta^2}$ and $\begin{cases} \text{A} = P_{\text{ref}} - P + \omega T_s Q \\ \text{B} = Q_{\text{ref}} - Q - \omega T_s P \end{cases}$.

The desired AC-side voltage vectors v_α and v_β can be calculated by formula (29), and the space vector modulation signal can be obtained.

In summary, the control block diagram of the three-phase Vienna rectifier system adopting the predictive power control strategy without grid voltage sensors is shown in Figure 8 To eliminate the steady-state error of the converter voltage v_{dc}, a

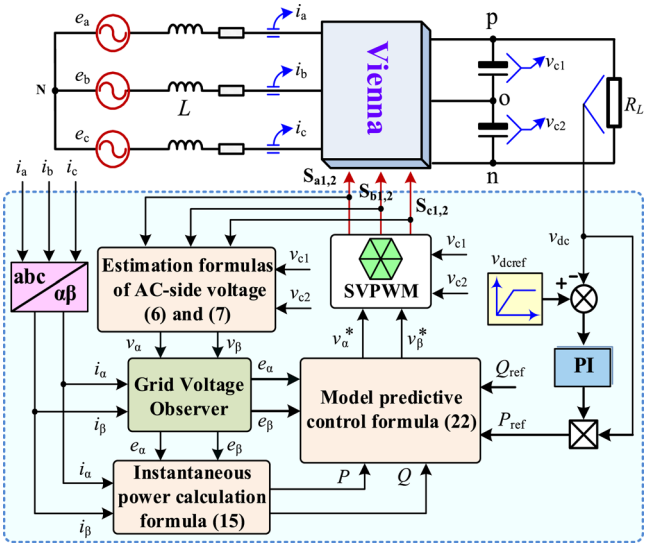

FIGURE 8 Control block diagram of predictive power control system.

PI regulator is used in outer loop to generate the active power reference value P_{ref}. According to the PI regulator, the P_{ref} can be expressed as:

$$P_{ref} = v_{dc}\left[(v_{dcref} - v_{dc})\left(k_p + \frac{k_i}{s}\right)\right] \tag{30}$$

The reactive power reference value Q_{ref} is set to zero to achieve unit power factor operation of the three-phase Vienna rectifier. Therefore, the symbols A and B in formula (29) can be redescribed as:

$$\begin{cases} A = v_{dc}\left[(v_{dcref} - v_{dc})\left(k_p + \frac{k_i}{s}\right)\right] - P + \omega T_s Q \\ B = -Q - \omega T_s P \end{cases}. \tag{31}$$

The resulting output voltage of the inverter can be explicitly observed from the final expression of formula (31).

6 | SIMULATION AND EXPERIMENTAL RESULTS

6.1 | Simulation analysis

A MATLAB/Simulink simulation model is established to verify the accuracy and effectiveness of the predictive power control strategy without grid voltage sensors of the three-phase Vienna rectifier, as proposed in this paper. The system parameters are presented in Table 2.

As shown in Figure 9, in a steady state, the actual and estimated waveform of the grid voltage in the two-phase stationary coordinate system align almost perfectly, illustrating the high estimation precision of the proposed grid voltage estimation algorithm.

TABLE 2 Simulation parameters of Vienna rectifier.

Parameters	Values
RMS value of the grid voltage E_m/V	220
Output voltage v_{dc}/V	700
Filter inductance L/mH	3.0
DC-side capacitors C_1, C_2/μF	2200
Switching frequency f_s/kHz	20
Current-limiting resistance $r_{start\text{-}up}$/Ω	40
Rated power /kW	10

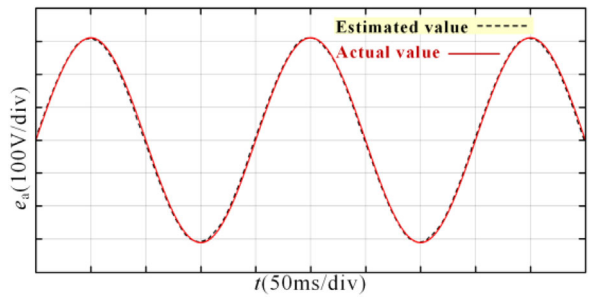

FIGURE 9 Actual value and estimated value of grid voltage in steady state.

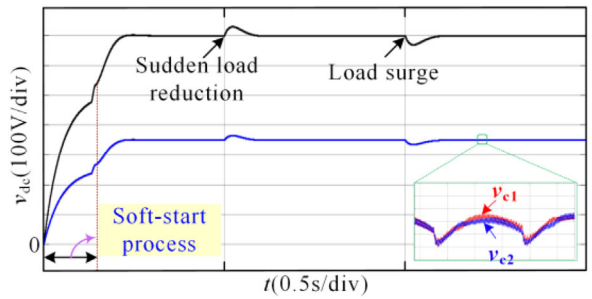

FIGURE 10 DC-side output voltage waveform.

The total simulation time is set as $t = 1.5$ s. When the system runs to 0.13 s, the system switches from uncontrolled rectification to PWM rectification mode; when it runs to 0.5 s, the output power is suddenly reduced from 10 to 5 kW; when it runs to 1 s, the output power is suddenly increased from 5 to 10 kW.

Figure 10 shows that after the pre-charging process is completed (10 kW), the output voltage reaches the reference value of 700 V stably with virtually no overshoot; when power is suddenly decreased (5 kW), overshoot is at 4.43% with an adjusted time of 55.6 ms; when power is rapidly increased (10 kW), voltage decreases by 4.28% with an adjustment time of 54.9 ms. The output voltage amplitude exhibits good dynamic performance and can be quickly adjusted to the reference value, while the waveform of DC-side capacitor voltage illustrates good output characteristics with no significant fluctuation in the neutral-point potential of the DC side.

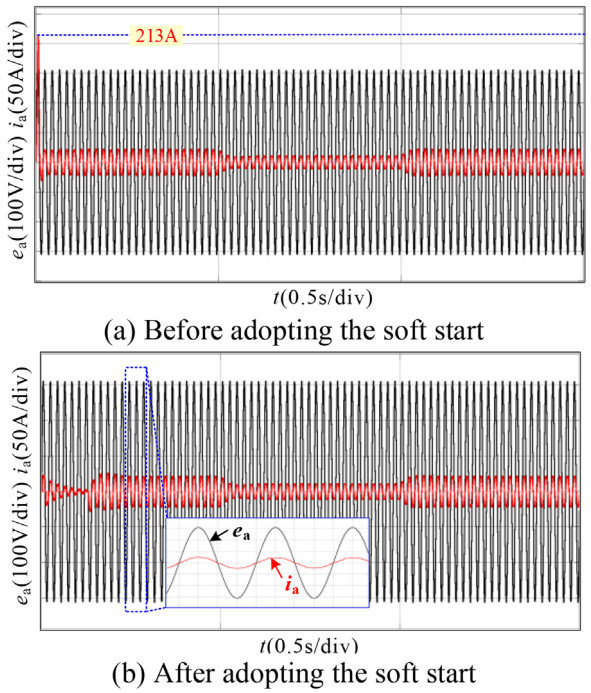

FIGURE 11 Waveform of phase-a grid voltage and current.

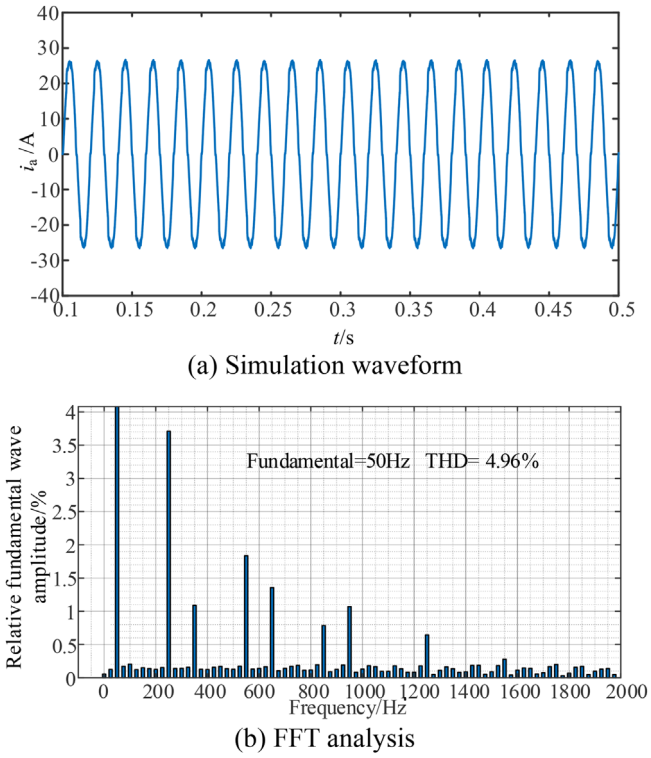

FIGURE 12 Simulation waveform and FFT analysis result of phase-a grid-side current under injecting fifth harmonic into the grid voltage.

Figure 11 shows the waveform of phase-a grid voltage and grid-side current before and after implementing the soft-start strategy. Without the soft-start strategy, the grid-side peak current reaches up to 213 A, while after adopting the soft-start strategy, the grid-side peak current decreases to 28 A, demonstrating the significant suppression effect on the impulse current. Moreover, the grid voltage and grid-side current maintain the same phase constantly, achieving unit power factor operation.

Figure 12a displays the phase-a grid-side current waveform when injecting a 15% fifth harmonic into the grid voltage. A slight distortion is observed in the current. Meanwhile, the FFT results depicted in Figure 12b demonstrate that the fifth harmonic content is 3.71%, and the THD value is 4.96% (<5%). These outcomes suggest that the proposed predictive power control strategy in this paper is minimally influenced by low-order harmonics of the grid voltage.

Figure 13 shows the simulation waveform of active power, reactive power, and power factor on the grid side of the rectifier throughout the load switching process.

As shown in Figure 13, the instantaneous active power of the rectifier can quickly and accurately track the reference value when the load is suddenly decreased and increased, whereas the reactive power remains stable at nearly zero. During steady-state operation, the power factor remains consistently above 0.95, effecting power factor correction.

Figure 14 shows the simulation waveforms under a phase voltage drop of 10%. Even if parameter mismatches surface in the grid voltage, advantageous performance can still be accomplished via predictive power control.

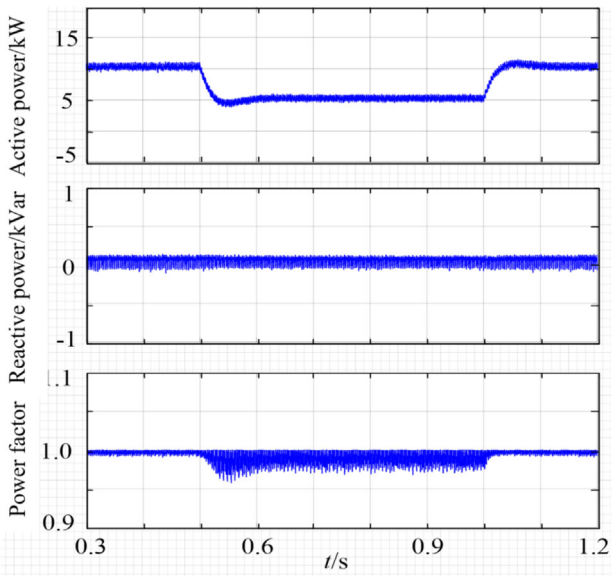

FIGURE 13 Active power, reactive power, and power factor.

6.2 | Experimental analysis

An experimental setup of a three-phase Vienna rectifier has been implemented to further validate the effectiveness of the proposed control strategy, as shown in Figure 15. The AC side of the rectifier is linked to a three-phase programmable grid simulator (Chroma 61830), whereas the DC output side is con-

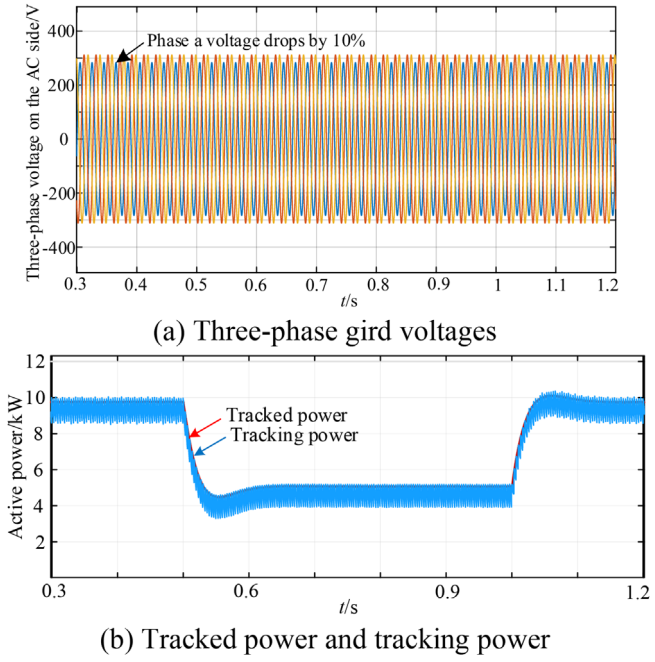

FIGURE 14 Simulation waveforms under a phase voltage drop of 10%.

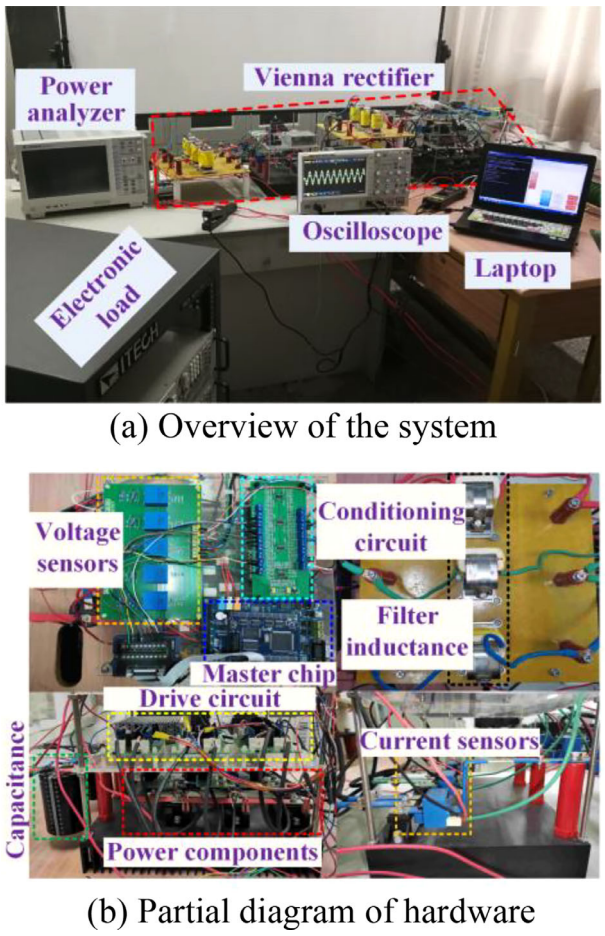

FIGURE 15 Experimental prototype of Vienna rectifier.

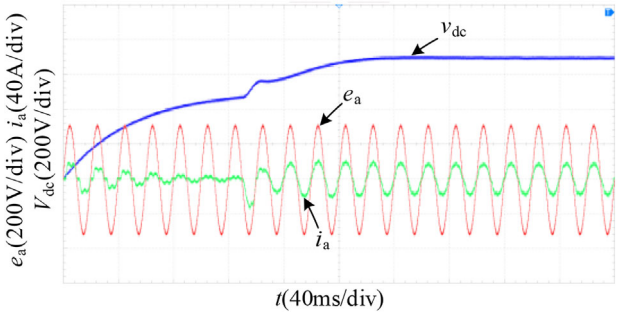

FIGURE 16 Experimental waveform during soft-start process.

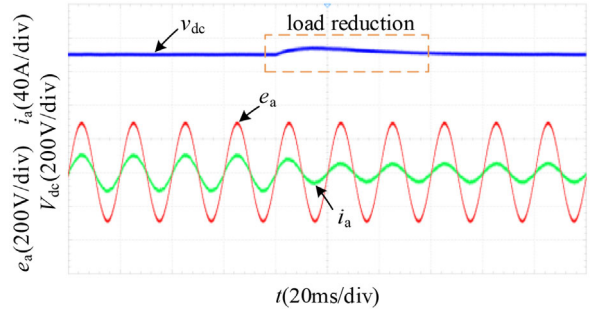

FIGURE 17 Dynamic experimental response to load step change.

nected to an electronic load (IETCH IT8018). The primary control chip used is TMS320F28335, while the power switch tubes and fast recovery diodes adopt an integrated module, MID75-12A3. The rectifier diodes comprise MDD56-12N1B, and the filter inductors are constructed with the amorphous alloy core AMCC-32. The current sensors are LEM HAS50, and the voltage sensors on the DC side are LEM LV25-P. The electrical parameters of the experimental prototype are congruous with the system simulation parameters.

Figure 16 shows the waveform of DC-side output voltage, phase-a grid-side voltage, and current during the starting process of a rectifier. It can be seen that the DC-side voltage smoothly rises to the reference voltage, and there is no large impulse current in the input current, which verifies the effectiveness of the soft-start method.

Figure 17 shows the waveform of DC-side output voltage, phase-a voltage, and input current when the load is switched.

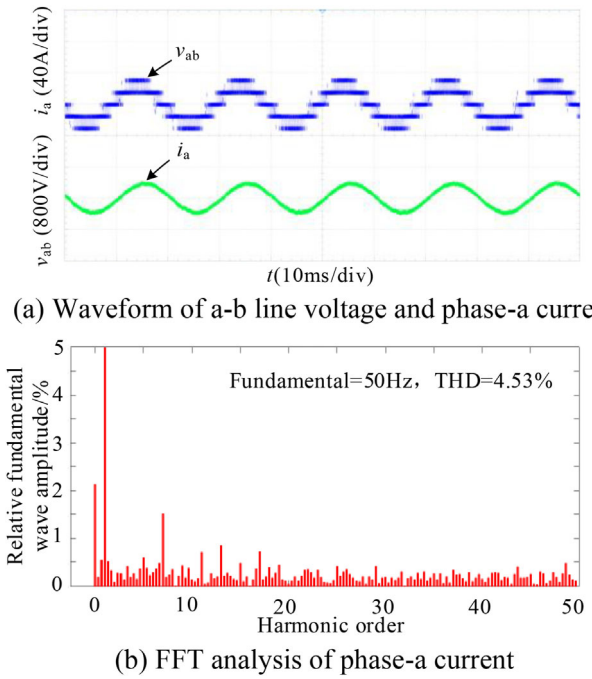

(a) Waveform of a-b line voltage and phase-a current

(b) FFT analysis of phase-a current

FIGURE 18 Steady-state experimental waveform at rated load.

It can be deduced from the waveform of the DC-side output voltage that the output voltage quickly returns to the reference value within three power frequency periods (60 ms) during the load switching processes. The system exhibits no static errors during steady-state operation and displays exceptional output characteristics. During the load dynamic switching and steady-state operation, the input current maintains a good sine degree and displays desirable input characteristics, consistent with the simulation results.

Figure 18 shows the waveform of line voltage (A–B) and phase-A current at the rated load. It can be seen that there is a $\pi/6$ phase difference between the line voltage and the phase current, and the line voltage is a typical five-level staircase wave.

During steady-state operation at rated load, the experimental data of phase-a input current was imported into MATLAB/Workspace for FFT analysis, as shown in Figure 18b. The analysis indicated that the THD value was 4.53% (<5%), meeting IEEE519 standard.

7 | CONCLUSIONS

This paper focus on the three-phase six-switch Vienna rectifier, proposing a grid voltage estimation algorithm and effectively combining it with predictive power control to form a predictive power control strategy without grid voltage sensors. A soft-start method is designed to effectively suppress the impulse current, aiming at the problem of difficult start-up caused by the impulse current of the Vienna rectifier in the actual system so that the rectifier can start smoothly and stably. Finally, the simulation and experimental verifications of the strategy show that the predictive power control strategy without grid voltage sensors proposed in this paper exhibits the following advantages:

1. The closed-loop control system formed without a grid voltage sensor exhibits good steady-state and dynamic performance.
2. The proposed grid voltage estimation algorithm is adaptable to voltage vector-oriented control strategy and can extend to other derivative topologies of the Vienna rectifier.

AUTHOR CONTRIBUTIONS

Tao Yang: Visualization; writing—original draft; writing—review and editing. **Lan Chen**: Investigation; methodology. **Yiru Miao**: Conceptualization; data curation.

ACKNOWLEDGEMENTS

This work is supported by the Science and Technology Research Program of Chongqing Municipal Education Commission (KJQN202203221) and the Doctoral Research Foundation of Chongqing Industry Polytechnic College (2022GZYBSZK1-04).

CONFLICT OF INTEREST STATEMENT

The authors declare no conflicts of interest.

DATA AVAILABILITY STATEMENT

The data that support the findings of this study are available from the corresponding author upon reasonable request.

ORCID

Tao Yang https://orcid.org/0000-0003-1860-2045

REFERENCES

1. Lee, J.S., Lee, K.B.: A novel carrier-based PWM method for Vienna rectifier with a variable power factor. IEEE Trans. Ind. Electron. 63(1), 3–12 (2016)
2. Adhikari, J., Prasanna, I.V., Panda, S.K.: Reduction of input current harmonic distortions and balancing of output voltages of the Vienna rectifier under supply voltage disturbances. IEEE Trans. Power Electron. 32(7), 5802–5812 (2017)
3. Li, X., Sun, Y., Wang, H., et al.: A hybrid control scheme for three-phase Vienna rectifiers. IEEE Trans. Power Electron. 33(1), 629–640 (2018)
4. Miao, Z., Tong, H., Jin, X., et al.: DQ-frame zero-crossing effect modeling and current distortion compensation method for Vienna rectifier. IEEE Trans. Power Electron. 35(7), 7612–7623 (2020)
5. M. Mehreganfar, M. H. Saeedinia, S. A. Davari, et al.: Sensorless predictive control of AFE rectifier with robust adaptive inductance estimation. IEEE Trans. Ind. Inf. 15(6), 3420–3431 (2019)
6. Noguchi, T., Tomiki, H., Kondo, S., et al.: Direct power control of PWM converter without power-source voltage sensors. IEEE Trans. Ind. Appl. 34(3), 473–479 (1998)
7. Guzman, R., DeVicuna, L., Morales, J., et al.: Model-based control for a three-phase shunt active power filter. IEEE Trans. Ind. Electron. 63(7), 3998–4007 (2016)
8. Kukkola, J., Hinkkanen, M.: State observer for grid-voltage sensorless control of a converter under unbalanced conditions. IEEE Trans. Ind. Appl. 54(1), 286–297 (2018)
9. Rahoui, A., Bechouche, A., Seddiki, H., et al.: Grid voltages estimation for three-phase PWM rectifiers control without ac voltage sensors. IEEE Trans. Power Electron. 33(1), 859–875 (2018)

10. Malinowski, M., Kazmierkowski, M. P., Hansen, S., et al.: Virtual flux based direct power control of three phase PWM rectifiers. IEEE Trans. Ind. Appl. 37(4), 1019–1027 (2001)
11. Zhang, H., Zhu, X., Shi, J., et al.: Study on PWM rectifier without grid voltage sensor based on virtual flux delay compensation algorithm. IEEE Trans. Power Electron. 34(1), 849–862 (2019)
12. Xiao, X., Zhang, Y., Song, X., et al.: Virtual flux direct power control for PWM rectifiers based on an adaptive sliding mode observer. IEEE Trans. Ind. Appl. 54(5), 5196–5205 (2018)
13. Shukla, S., Singh, B.: Single-stage PV-grid interactive induction motor drive with improved flux estimation technique for water pumping with reduced sensors. IEEE Trans. Power Electron. 35(12), 12988–12999 (2020)
14. Prakash, P. S., Kalpana, R., Singh, B., et al.: Design and implementation of sensorless voltage control of front-end rectifier for power quality improvement in telecom system. IEEE Trans. Ind. Appl. 54(3), 2438–2448 (2018)
15. Mukherjee, D., Kastha, D.: Voltage sensorless control of Vienna rectifier in the input current oriented reference frame. IEEE Trans. Power Electron. 34(8), 8079–8091 (2019)
16. Kumar, A., Srungavarapu, G.: A power quality enhanced grid voltage sensorless predictive direct power control for active front end rectifiers. Trans. Inst. Meas. Control 40(13), 3809–3823 (2018)
17. Yang, H., Zhang, Y., Liang, J., et al.: Sliding-mode observer based voltage-sensorless model predictive power control of PWM rectifier under unbalanced grid conditions. IEEE Trans. Ind. Electron. 65(7), 5550–5560 (2018)
18. Mehreganfar, M., Saeedinia, M.H., Davari S A, et al.: Sensorless predictive control of AFE rectifier with robust adaptive inductance estimation. IEEE Trans. Ind. Inf. 15(6), 3420–3431 (2019)
19. Upamanyu, K., Ameta, C., Narayanan, G.: Simplified input voltage sensorless vector control for PWM rectifiers. IEEE Trans. Ind. Appl. 56(4), 4051–4060 (2020)
20. Kumar, M., Huber, L., Jovanovic, M.M.: Start-up procedure for DSP-controlled three-phase six-switch boost PFC rectifier. IEEE Trans. Power Electron. 30(8), 4514–4523 (2015)
21. Gu, B.G., Choi, J.H., Jung, I.S.: Start-up current control method for three phase PWM rectifiers with a low initial dc link voltage. J. Power Electron. 12(4), 587–594 (2012)
22. Liu, T., Xia, C., Shi, T.: Robust model predictive current control of grid-connected converter without alternating current voltage sensors. IET Power Electron. 7(12), 2934–2944 (2014)
23. Kumar, M., Huber L., Jovanović, M.M.: Start-up procedure for DSP-controlled three-phase six-switch boost PFC rectifier. IEEE Trans. Power Electron. 30(8), 4514–4523 (2015)

How to cite this article: Yang, T., Chen, L., Miao, Y.: Predictive power control strategy without grid voltage sensors of the Vienna rectifier. IET Power Electron. 17, 1411–1421 (2024). https://doi.org/10.1049/pel2.12707